JOURNAL OF COMPUTATIONAL PHYSICS 47, 331–351 (1982)

Coordinate Generation with Precise Controls over Mesh Properties

PETER R. EISEMAN*

Department of Applied Physics and Nuclear Engineering, Columbia University, New York, New York 10027

Received December 17, 1980; revised November 20, 1981

Coordinate generation techniques with precise controls over mesh properties are mathematically developed. The controls are precise because mesh properties can be explicitly specified within a local region independent of the mesh elsewhere. The local regions can adjoin boundaries where a particular mesh form can greatly simplify a problem or can be used for a smooth juncture between distinct coordinate systems where, in effect, a branch cut with a prescribed geometry and mesh distribution can be obtained. Away from boundaries, a local region can be given a particular mesh form to model internal objects or to simplify a problem.

INTRODUCTION

The numerical solution of boundary value problems over complicated domains often requires the application of a mesh generation algorithm in which specifications of mesh properties are possible. Such properties include boundary specifications (for geometry, pointwise distributions, mesh angles, and rates of entry), uniformity specifications (for either local or global distributions of coordinate curves or points), and specifications for numerous interior properties such as the smooth (i.e., with continuous derivatives) embedding of a Cartesian system within a global mesh. The boundary specifications are useful when coordinate systems are to be smoothly assembled to form a well-ordered composite mesh; mesh uniformity is necessary when points or curves are to be redistributed by an a priori specification of a distribution function or by a solution adaptive approach, both without any distortion from the underlying transformation; and finally, when an interior form such as Cartesian or polar would simplify the form of the equations to be solved.

To generate a mesh with specified properties, transformations of a general type must be considered. In this context, conformal transformations are too restrictive since a specified distribution of boundary points generally could not be given in

* Research was performed under AFOSR Contrast No. F49620–79–C–0132. Partial support was supplied under NASA Contract No. NAS1–15810 while the author was in residence at the Institute for Computer Applications in Science and Engineering (ICASE), NASA Langley Research Center, Hampton, VA 23665.

0021-9991/82/090331–21$02.00/0

advance because of the analytic continuation properties of analytic functions. Examples of some of the most developed conformal techniques are given by Ives [1] and by Davis [2]. To admit arbitrary boundary distributions, nonorthogonal transformations were considered. The first general approach was to specify both the boundary geometry and pointwise distributions as boundary conditions for a system of elliptic partial differential equations of the Poisson type [3, 4]. In addition, periodic conditions resulted in the capability to make branch cuts, and consequently, to make some composite systems [5, 6]. The smooth junctures (branch cuts) between such systems, however, could not be simply prescribed in advance: a simple prescription would require Dirichlet boundary conditions, and hence, derivative discontinuities along the cut [7, 8]. In this context, the creation of extra boundary conditions would be less successful since an increase in the order of the system would be required; as a result, the previous guarantee of nonsingularity would be lost. Consequently, the only remaining possibility is an algorithm for the selection of the forcing functions, such as the study pursued with some success by Steger and Sorenson [9]. The simultaneous specification of further mesh properties, beyond that considered by Steger and Sorenson, is extremely limited with methods based upon Poisson equations.

In a subsequent general approach to the mesh generation problem, the additional specifications of mesh properties became possible with the development of the multisurface method [10] which extended earlier work on coordinates for cascades of turbine blades [11]. With the multisurface method, intermediate control surfaces are introduced between bounding surfaces so that the mesh properties can be naturally prescribed by parametric alignment. In particular, the control surfaces, which should not be mistaken for coordinate surfaces, define a discrete vector field which is interpolated, integrated, and normalized to obtain the desired transformation. In the basic multisurface study [10], only polynomial interpolates were considered. The resulting transformations provided all of the desired boundary specifications for the form of the mesh without the necessity for solving differential equations. An automatic algorithm based upon the multisurface transformation also has an advantage with dimensionality since n-dimensional coordinates are constructed from only $(n-1)$- and 1-dimensional surfaces. As a consequence, the advantage is in computational speed and storage. In addition, special cases can be specified analytically, should that prove to be more convenient or more conservative of computer storage. One such case was the three-dimensional coordinate system about wings presented in [12].

In the present study, the multisurface transformation is derived with interpolants each of which vanishes identically outside of a small region around its corresponding point of interpolation. These local interpolants then lead directly to precise local controls on the form of the mesh both along the boundaries and internally. Although local controls are available with methods based upon Poisson equations and with the polynomial version of the multisurface transformation, the capability for precise internal specifications are not. As an example of the desired degree of precision, a region with curved boundaries can be transformed in such a way that most of the interior is covered by a uniform Cartesian mesh which need not be rectangular. A

discrete representation of a boundary value problem over the region would then smoothly change from a fully curvilinear form to a simpler Cartesian form over most of the mesh area.

The general multisurface transformation of [10] is given with arbitrary interpolation functions in a preliminary section where the interpolation functions are used to establish a smooth vector field tangent to a desired family of coordinate curves. Part or all of the coordinate curves in the family can be given a uniform distribution, provided that the interpolants are properly chosen. Conditions for the admissibility of uniformity are then derived for the general interpolation functions. From this stage, particular local interpolation functions which satisfy the admissibility condition are constructed and examined for various levels of derivative continuity. In the present study, the functions are only required to be in the continuity class of C^0 functions where 0 indicates the highest continuous derivative. In particular, these functions are piecewise linear functions which are relatively easy to examine. The resulting transformation has continuous first derivatives and consequently belongs to class C^1. Rather than a direct progression to higher levels of derivative continuity, a short sequence of two-dimensional examples are presented herein to explicitly demonstrate the power of local methods. In a companion study [13], higher level continuity is developed. The increased level is needed to extend the range of applications. Of particular importance is the extension to the general case in three dimensions, where C^2 continuity is a minimum requirement to insure that coordinate curves bend continuously, not abruptly.

The Multisurface Transformation

When curvilinear coordinates are employed in the numerical solution of a boundary value problem, constraints must often be placed upon the coordinates, in addition to the basic requirement that the bounding surfaces are coordinate surfaces of one or more coordinate systems. The locations of the constraints can occur anywhere in the problem domain. On the boundaries, a particular pointwise distribution may be needed; in regions near boundaries, a particular coordinate form may be advantageous; and away from the boundaries, an internal coordinate specification may also be required. Typically, the constraints will arise either to resolve regions with large solution gradients or to cause some simplification in the problem formulation and solution.

In conjunction with the demand for constraints, methods for generating coordinates have been developed to meet the demand. One of the most flexible methods for this purpose is the multisurface method presented in [10]. The full level of flexibility, however, was not entirely exploited in [10], since the emphasis was placed upon global methods which gave more control near boundaries and less internally. In the present study, local methods will be developed within the context of the general multisurface transformation. The result will be precise local controls which are applicable anywhere in the problem domain.

As a preliminary to the present study, the general multisurface transformation must be examined. The multisurface transformation is a method for coordinate generation between an inner bounding surface $\mathbf{P}_1$ and an outer bounding surface $\mathbf{P}_N$. To establish a particular distribution of mesh points on each bounding surface, a common parameterization $\mathbf{t}$ is chosen for each surface. This is equivalent to a coordinate description of the surfaces which yields the desired surface mesh when the parametric components of $\mathbf{t}$ are given a *uniform* discretization. With the parametric description, the inner and outer bounding surfaces are denoted by $\mathbf{P}_1(\mathbf{t})$ and $\mathbf{P}_N(\mathbf{t})$, respectively. At this stage, coordinates could be generated along the straight line segments connecting points of common parametric value of each bounding surface [11]. In continuation, parameterized intermediate surfaces $\mathbf{P}_2(\mathbf{t}),\ldots, \mathbf{P}_{N-1}(\mathbf{t})$ are introduced so that they can be used as controls over the internal form of the coordinates. The intermediate surfaces are not coordinate surfaces, but instead are surfaces that are used to establish a vector field that is composed of tangent vectors to the coordinate curves spanning the coordinate system to connect bounding surfaces. It is also assumed that the collection of surfaces $\mathbf{P}_1(\mathbf{t})$, $\mathbf{P}_2(\mathbf{t}),\ldots,$ $\mathbf{P}_N(\mathbf{t})$ is ordered from bounding surface to bounding surface. An illustration is given in Fig. 1. For a fixed parameter value $\mathbf{t}$, there is a corresponding point on each surface. The piecewise linear curve obtained by connecting corresponding points is given by the dashed curve in Fig. 1. From the figure, it can be observed that the tangent directions determined by the piecewise linear curve are piecewise constants. As $\mathbf{t}$ is varied, the field of tangent directions

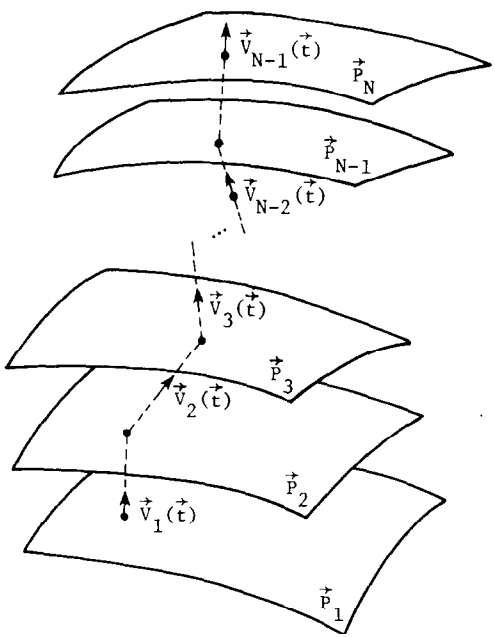

FIG. 1. A piecewise linear curve and its tangent field.

obtain their smoothness only in **t**. To obtain smoothness in going from bounding surface to bounding surface, a sufficiently smooth interpolation must be performed. The result is a smooth vector field of undetermined magnitude which gives the desired tangential directions for coordinate curves connecting the bounding surfaces. A unique vector field of tangents is then obtained by correctly choosing magnitudes so that, on integration, the bounding surfaces are fit precisely.

In symbols, a vector field tangent to the piecewise linear curves is given by $\mathbf{V}_k(\mathbf{t}) = A_k|\mathbf{P}_{k+1}(\mathbf{t}) - \mathbf{P}_k(\mathbf{t})|$ between the kth and $(k+1)$th surfaces, where k is taken to vary (if $N > 2$) from the first bounding surface to the final intermediate surface. These vectors are indicated in Fig. 1. The coefficients A_k are scalars which determine the magnitude of the vectors but not the directions. An independent variable r is assumed for the spanning direction. A vector valued function which is discrete in r can now be defined as a map from r_k into $\mathbf{V}_k$ for a partition $r_1 < r_2 < \cdots < r_{N-1}$ and for $k = 1,..., N-1$. A sufficiently smooth vector field $\mathbf{V}(r, \mathbf{t})$ is then obtained by a sufficiently smooth interpolation $\mathbf{V}(r_k, \mathbf{t}) = \mathbf{V}_k(\mathbf{t})$. With r as a continuous independent variable, the r derivative of the coordinate transformation $\mathbf{P}(r, \mathbf{t})$ is equal to the interpolant. Specifically,

$$\frac{\partial \mathbf{P}}{\partial r} = \mathbf{V} = \sum_{k=1}^{N-1} \psi_k(r)\, \mathbf{V}_k(\mathbf{t}), \tag{1}$$

where $\psi_k(r_j)$ is unity at $k = j$ and vanishes otherwise. Since the coordinate transformation must be obtained from an integration in the r variable, the interpolant ψ_k must be continuously differentiable up to an order which is one less than the level of smoothness desired for the coordinates. The construction of the local controls mentioned above will rely heavily upon the development of suitably smooth interpolation functions. If the integral of Eq. (1) has a constant of integration equal to $\mathbf{P}_1(\mathbf{t})$ and if the quantities $A_k \psi_k(r)$ integrate to unity over the domain $r_1 \leqslant r \leqslant r_{N-1}$, then a coordinate transformation which matches the desired bounding surfaces is obtained. This transformation is called a multisurface transformation since, in addition to bounding surfaces, it also uses a collection of surfaces which are not coordinate surfaces, but which instead are surfaces that can be used to control the form of the coordinates throughout the domain. The multisurface transformation is then explicitly given by

$$\mathbf{P}(r, \mathbf{t}) = \mathbf{P}_1(\mathbf{t}) + \sum_{k=1}^{N-1} \frac{G_k(r)}{G_k(r_{N-1})} |\mathbf{P}_{k+1}(\mathbf{t}) - \mathbf{P}_k(\mathbf{t})|, \tag{2a}$$

where

$$G_k(r) = \int_{r_1}^{r} \psi_k(x)\, dx, \tag{2b}$$

for $k = 1, 2, \ldots, N-1$. Due to the normalization conditions on the A_k, the original semidiscrete vector field, illustrated in Fig. 1, is given by

$$\mathbf{V}_k(\mathbf{t}) = (1/G_k(r_{N-1}))[\mathbf{P}_{k+1}(\mathbf{t}) - \mathbf{P}_k(\mathbf{t})], \tag{3}$$

for $k = 1, 2, \ldots, N-1$.

A Uniform Distribution of Coordinate Surfaces

The distribution of any set of objects is most accurately specified relative to uniform conditions. When the objects are points on a straight line segment and when uniform conditions are represented by an arc length parameterization S, a substitution of a distribution function $S(x)$ will directly distribute points along the line relative to distance. In a discrete sense, a uniform mesh in x corresponds with an appropriately distributed mesh on the line. When the objects to be distributed, however, are families of coordinate surfaces rather than isolated points, the measure of uniformity and its determination is more complex. In spite of the potential complexities, it is possible to define a measure of uniformity and to determine appropriate conditions in a relatively simple manner for the multisurface transformation (Eq. (2)).

With the multisurface transformation, uniformity can be defined and obtained for the family of coordinate surfaces determined by constant values of the variable r. Relative to the uniform distribution of the constant r coordinate surfaces, a distribution function $r(x, \mathbf{t})$ can be directly applied without any distortion from the basic underlying multisurface transformation $\mathbf{P}(r, \mathbf{t})$, given in Eq. (2). The transformation with distribution is then given by the composition $\mathbf{P}(r(x, \mathbf{t}), \mathbf{t})$ with a new variable x. Both the uniformity and the distribution function can be defined either globally or locally. In the global case which was studied in [10], uniformity conditions were imposed on the underlying transformation as the constant r coordinate surfaces are taken from bounding surface to bounding surface. By contrast, in the local case, a particular local coordinate form can be specified from constant r coordinate surfaces, where the domain of r is restricted to a specified region.

For both local and global uniformity, a smooth vector field $\boldsymbol{\tau}(\mathbf{t})$ is specified to define directions in which uniformity can be measured for each value of $\mathbf{t}$. The measurement is given by the dot product

$$S_p(r, \mathbf{t}) = [\mathbf{P}(r, \mathbf{t}) - \mathbf{P}_1(\mathbf{t})] \cdot \boldsymbol{\tau}(\mathbf{t}) \tag{4}$$

which is a projection of a coordinate curve in the r variable onto the direction given by $\boldsymbol{\tau}(\mathbf{t})$. Since S_p is just a distance along $\boldsymbol{\tau}(\mathbf{t})$, it can be called a projected arc length. In a very real sense, the various measurements of distance in the various directions can be viewed as if a collection of yardsticks were used for such measurements

between points corresponding to $\mathbf{t}$ as $\mathbf{t}$ varied. From a substitution of the multisurface transformation (Eq. (2)), the projected arc length becomes

$$S_p(r, \mathbf{t}) = \sum_{k=1}^{N-1} \frac{G_k(r)}{G_k(r_{N-1})} C_k(\mathbf{t}), \tag{5a}$$

where

$$C_k(\mathbf{t}) = [\mathbf{P}_{k+1}(\mathbf{t}) - \mathbf{P}_k(\mathbf{t})] \cdot \boldsymbol{\tau}(\mathbf{t}) \tag{5b}$$

is the projection of the kth discrete tangent vector onto the vector field direction.

When the projected arc length is linear in r for a range of $\mathbf{t}$ values, the distribution of constant r coordinate surfaces will be uniform relative to the vector field $\boldsymbol{\tau}(\mathbf{t})$. When linearity exists only for a limited range of r, the uniformity will be valid only locally, as opposed to a global uniformity valid for all values of r. To establish a good measure for uniformity, the selected vector field directions must be well aligned with the variable r coordinate curves or the parts of those curves where uniformity is to be considered. A readily available class of vector fields which are well aligned either locally or globally is given by

$$\boldsymbol{\tau}_{ijk}(\mathbf{t}) = (\mathbf{P}_i(\mathbf{t}) - \mathbf{P}_j(\mathbf{t}))/\|\mathbf{P}_i(\mathbf{t}) - \mathbf{P}_j(\mathbf{t})\|^k, \tag{6}$$

where $1 \leqslant j < i \leqslant N$. When $\boldsymbol{\tau}(\mathbf{t}) = \boldsymbol{\tau}_{N12}(\mathbf{t})$ is inserted into Eq. (4) and when linearity is imposed, the global uniformity conditions studied in [10] for the cases with polynomial interpolation functions are obtained. The choice $k = 2$ resulted in a normalization of projected arc lengths to all lie within the internal $|r_1, r_{N-1}|$, and as such was a convenience since uniformity reduced to $S_p = (r - r_1)/(r_{N-1} - r_1)$. An illustration of this global case is given in Fig. 2. If k had been set to unity, then

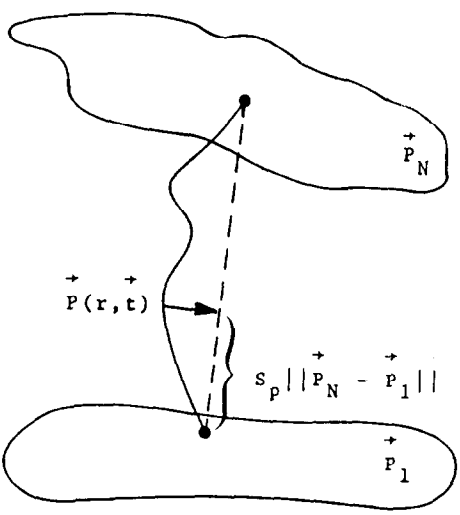

FIG. 2. A projected arc length for global uniformity.

uniformity would have been given by $S_p = \|\mathbf{P}_N - \mathbf{P}_1\|(r - r_1)/(r_{N-1} - r_1)$, reflecting the actual rather than relative distances. This latter choice will be preferred when local uniformity is considered, since actual distances would be less confusing.

In the general case, the uniformity condition is given by

$$S_p(r, \mathbf{t}) = b(\mathbf{t})(r - r_1)/(r_{N-1} - r_1), \tag{7}$$

where $b(\mathbf{t})$ is determined by the choice of $\tau(\mathbf{t})$. To satisfy the uniformity condition of Eq. (7), suitable choices for the $N-1$ discrete projections $C_k(\mathbf{t})$ of Eq. (5b) must be determined. By function evaluation at each of the partition points, a coupled system of $N-1$ independent equations is obtained from Eq. (7). Although the coupled system could be solved with some linear algebra, the same solution can be obtained by a direct observation of the derivative equation

$$\frac{\partial S_p}{\partial r} = \sum_{k=1}^{N-1} \frac{\psi_k(r)}{G_k(r_{N-1})} C_k(\mathbf{t}), \tag{8}$$

which is equivalent to Eq. (5) when the initialization $S_p(r_1, \mathbf{t}) = 0$ is applied. Since the interpolation functions satisfy a cardinality condition $\psi_i(r_j) = A_i \delta_{ij}$ for some constants A_i, the uniformity condition in differentiated form collapses to an equation with just one term on each side. The immediately observed solution is then given by

$$C_k(\mathbf{t}) = b(\mathbf{t})\, G_k(r_{N-1})/(r_{N-1} - r_1)\, \psi_k(r_k), \tag{9}$$

for $k = 1, 2, \ldots, N-1$. As an example, the uniformity conditions of [10] are also contained in Eq. (9). When Eqs. (7) and (9) are inserted into Eq. (8) and when $b(\mathbf{t})/(r_{N-1} - r_1)$ is divided out of both sides of the resulting equation, the uniformity constraint

$$\sum_{k=1}^{N-1} \frac{\psi_k(r)}{\psi_k(r_k)} = 1, \tag{10}$$

is obtained. By a parallel analysis, this constraint is also seen to be valid in the slightly more general case where the origin $\mathbf{P}_1(\mathbf{t})$ in Eq. (4) is replaced by an arbitrary vector field dependent only upon $\mathbf{t}$. In summary, one has

THEOREM 1. *For uniformity to be possible either locally or globally, the interpolation functions must be chosen to satisfy Eq.* (10). *When the interpolation functions satisfy Eq.* (10), *uniformity can be specified by a selection of intermediate control surfaces in such a way that the discrete projections of Eq.* (5b) *are given by Eq.* (9).

LOCAL C^0 INTERPOLATION FUNCTIONS

The multisurface transformation (Eq. (2)) is defined locally when the interpolation functions ψ_k are chosen to vanish outside of a small interval. The advantage inherent in the local definitions is that the coordinates can be manipulated in a local region without causing a concurrent ripple effect that would change coordinates elsewhere, as would occur with global methods. The local manipulations, moreover, can be done in a precise fashion and consequently, lead to precise controls over the coordinates. The coordinates have a level of smoothness which, due to the multisurface integration (Eq. (2b)), is one level of differentiability higher than that specified for the interpolation functions. In particular, if the interpolants belong to the class C^m of functions which have continuous mth order derivatives then the multisurface transformation belongs to class C^{m+1} when the surfaces $\mathbf{P}_k(\mathbf{t})$ also belong to class C^{m+1}. In general, the complexity of the interpolants increases when the level of smoothness is increased. Consequently, it is best to use the least amount of smoothness that is permissable for a given problem. In fact, a large percentage of the potential applications can be studied with either C^0 or C^1 interpolants.

The simplest local interpolants belong to the class C^0 of continuous functions and are defined by linear segments. An illustration of these continuous piecewise linear interpolation functions is given in Fig. 3. On examination of the multisurface transformation (Eq. (2)), the height $\psi_k(r_k)$ of the interpolation functions is seen to be arbitrary since a change of scale by multiplication with any real number would not change the transformation. For algebraic simplicity, each $\psi_k(r_k)$ will then be set to unity and the notation $h_k = r_{k+1} - r_k$ will be used for $k = 1, 2, \ldots, N-2$. With the specific heights, the algebraic expressions for the interpolation functions are given by

$$\begin{aligned} \psi_1(r) &= (r_2 - r)/h_1, && \text{for} \quad r_1 \leqslant r < r_2, \\ &= 0, && \text{for} \quad r_2 \leqslant r \leqslant r_{N-1}, \end{aligned} \tag{11a}$$

$$\begin{aligned} \psi_k(r) &= 0, && \text{for} \quad r_1 \leqslant r < r_{k-1}, \\ &= (r - r_{k-1})/h_{k-1}, && \text{for} \quad r_{k-1} \leqslant r < r_k, \\ &= (r_{k+1} - r)/h_k, && \text{for} \quad r_k \leqslant r < r_{k+1}, \\ &= 0, && \text{for} \quad r_{k+1} \leqslant r \leqslant r_{N-1}, \end{aligned} \tag{11b}$$

for $2 \leqslant k \leqslant N-2$; and

$$\begin{aligned} \psi_{N-1}(r) &= 0, && \text{for} \quad r_1 \leqslant r < r_{N-2}, \\ &= (r - r_{N-2})/h_{N-2}, && \text{for} \quad r_{N-2} \leqslant r \leqslant r_{N-1}. \end{aligned} \tag{11c}$$

One may also note that the C^0 interpolation functions are B-splines [14] of degree 1. In the C^1 case considered separately in Eiseman [13], B-splines will not work for

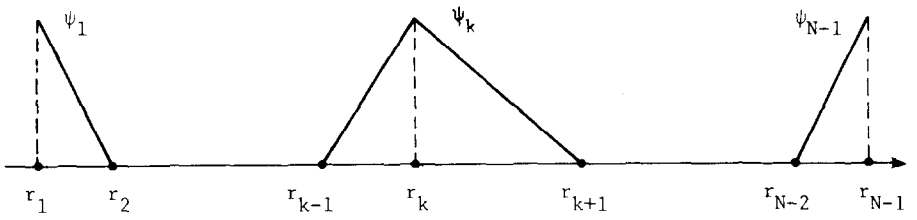

FIG. 3. Continuous piecewise linear interpolation functions.

reasons that will be clear when the C^1 developement is undertaken. By a direct substitution from Eq. (11), the integrals (Eq. (2b)) for the multisurface transformation are given by

$$\begin{aligned} G_1(r) &= (h_1/2) - (1/2h_1)(r_2 - r)^2, && \text{for } r_1 \leqslant r < r_2, \\ &= h_1/2, && \text{for } r_2 \leqslant r \leqslant r_{N-1}, \end{aligned} \tag{12a}$$

$$\begin{aligned} G_k(r) &= 0, && \text{for } r_1 \leqslant r < r_{k-1}, \\ &= (1/2h_{k-1})(r - r_{k-1})^2, && \text{for } r_{k-1} \leqslant r < r_k, \\ &= ((h_k + h_{k-1})/2) - \\ &\qquad (1/2h_k)(r_{k+1} - r)^2, && \text{for } r_k \leqslant r < r_{k+1}, \\ &= (h_k + h_{k-1})/2, && \text{for } r_{k+1} \leqslant r \leqslant r_{N-1}, \end{aligned} \tag{12b}$$

for $2 \leqslant k \leqslant N - 2$; and

$$\begin{aligned} G_{N-1}(r) &= 0, && \text{for } r_1 \leqslant r < r_{N-2}, \\ &= (1/2h_{N-2})(r - r_{N-2})^2, && \text{for } r_{N-2} \leqslant r \leqslant r_{N-1}. \end{aligned} \tag{12c}$$

A graphical illustration of the functions from Eq. (12) is given in Fig. 4. Each function increases from 0 to a maximum saturation value which is precisely the normalization value in the multisurface transformation, Eq. (2a). When the functions in Fig. 4 are given the normalization, the functional shape remains unaltered, but the saturation value becomes unity. On the interval $r_m \leqslant r < r_{m+1}$, the effect of the saturation values is to cause a telescopic collapse of $\mathbf{P}_1(\mathbf{t})$ and the first $m - 2$ terms of the sum in Eq. (2a). The last terms in the sum, starting with $k = m + 1$ and going up to $k = N - 1$, simply do not appear since their values are 0. Consequently, on the interval $r_m \leqslant r < r_{m+1}$, the multisurface transformation reduces to the local form

$$\begin{aligned} \mathbf{P}(r, \mathbf{t}) = \mathbf{P}_m(\mathbf{t}) &+ \frac{G_m(r)}{G_m(r_{N-1})} [\mathbf{P}_{m+1}(\mathbf{t}) - \mathbf{P}_m(\mathbf{t})] \\ &+ \frac{G_{m+1}(r)}{G_{m+1}(r_{N-1})} [\mathbf{P}_{m+2}(\mathbf{t}) - \mathbf{P}_{m+1}(\mathbf{t})], \end{aligned} \tag{13}$$

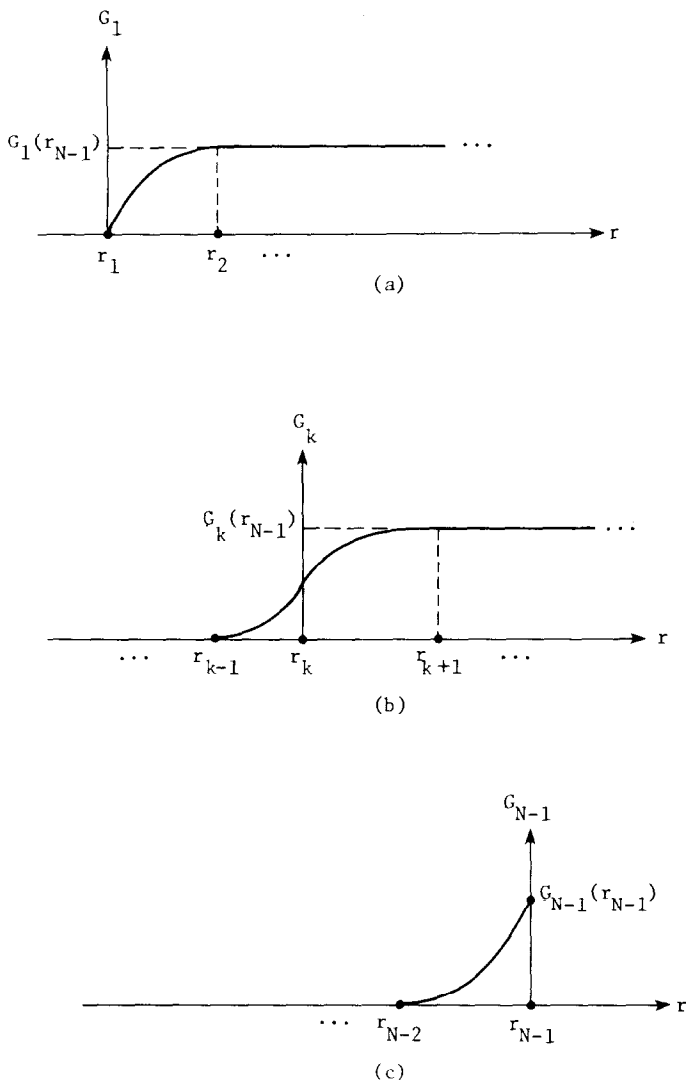

FIG. 4. Integrals of the C^0 interpolation functions from Fig. 3.

which is valid for $m = 1, 2, \ldots, N-2$ and was anticipated by the local construction of interpolation functions. Since the interpolants are not differentiable at the partition points r_k, the coordinate curves in the r variable usually have second derivative discontinuities, hence curvature and torsion (cf. [15]) discontinuities, at partition points. Since torsion is a measure of the rate at which a curve will be nonplanar, a torsion discontinuity would lead to a kink in a curve in three-dimensional space. The torsion discontinuities, however, can be removed by considering only curves in two dimensions, in which case torsion vanishes identically. Consequently, for the C^0

interpolants, the applications will be restricted to two dimensions and the scalar parameterization $\mathbf{t} = t$ will be assumed for Eq. (13).

With the two-dimensional parameterization, the evaluation of the transformation (Eq. (13)) at partition points is given by

$$\mathbf{P}(r_1, t) = \mathbf{P}_1(t), \tag{14a}$$

$$\mathbf{P}(r_m, t) = [h_m/(h_{m-1} + h_m)]\,\mathbf{P}_m(t) + [h_{m-1}/(h_{m-1} + h_m)]\,\mathbf{P}_{m+1}(t), \tag{14b}$$

for $2 \leqslant m \leqslant N - 2$, and by

$$\mathbf{P}(r_{N-1}, t) = \mathbf{P}_N(t). \tag{14c}$$

When $m = 1$ or $N - 1$, the respective bounding surfaces are fit as expected; and when m is between 1 and $N - 1$, the evaluation lies on the line segment between $\mathbf{P}_m(t)$ and $\mathbf{P}_{m+1}(t)$ since the coefficients each belong to the unit interval and add up to unity. Consequently, the vector differences in the transformation (Eq. (13)) can be rewritten as scaled differences between $\mathbf{P}_{m+1}(t)$ and the evaluations at r_m and r_{m+2}, respectively. When $\mathbf{P}_{m+1}(t)$ is obtained from Eq. (14b) and $\mathbf{P}_m(t)$ is subtracted from the result, one has

$$\mathbf{P}_{m+1}(t) - \mathbf{P}_m(t) = (1 + (h_m/h_{m-1}))[\mathbf{P}_{m+1}(t) - \mathbf{P}(r_m, t)], \tag{15a}$$

and similarly, one has

$$\mathbf{P}_{m+2}(t) - \mathbf{P}_{m+1}(t) = (1 + (h_m/h_{m+1}))[\mathbf{P}(r_{m+1}, t) - \mathbf{P}_{m+1}(t)], \tag{15b}$$

when Eq. (14b) with m replaced by $m + 1$ is solved for $\mathbf{P}_{m+1}(t)$ and subtracted from $\mathbf{P}_{m+2}(t)$. The equations are simultaneously valid when $3 \leqslant m + 1 \leqslant N - 3$. Otherwise, an endpoint evaluation occurs and the original difference would remain unchanged. By an addition and subtraction of the first difference in Eq. (13), the transformation can be centered locally about $\mathbf{P}_{m+1}(t)$, thus replacing $\mathbf{P}_m(t)$. From substitutions of Eqs. (14a), (15), ad (14c) into the locally centered forms, the transformation is expressed by

$$\begin{aligned}\mathbf{P}(r, t) = \mathbf{P}_2(t) &- [1 - (G_1(r)/G_1(r_{N-1}))][\mathbf{P}_2(t) - \mathbf{P}(r_1, t)] \\ &+ (1 + (h_2/h_1))(G_2(r)/G_2(r_{N-1}))[\mathbf{P}(r_2, t) - \mathbf{P}_2(t)],\end{aligned} \tag{16a}$$

for $r_1 \leqslant r < r_2$;

$$\begin{aligned}\mathbf{P}(r, t) = \mathbf{P}_{m+1}(t) &- (1 + (h_{m-1}/h_m))[1 - (G_m(r)/G_m(r_{N-1}))][\mathbf{P}_{m+1}(t) - \mathbf{P}(r_m, t)] \\ &+ (1 + (h_{m+1}/h_m))(G_{m+1}(r)/G_{m+1}(r_{N-1}))[\mathbf{P}(r_{m+1}, t) - \mathbf{P}_{m+1}(t)],\end{aligned} \tag{16b}$$

for $r_m \leqslant r < r_{m+1}$, $2 \leqslant m \leqslant N-2$; and

$$\mathbf{P}(r,t) = \mathbf{P}_{N-1}(t) - (1 + (h_{N-3}/h_{N-2}))[1 - (G_{N-2}(r)/G_{N-2}(r_{N-1}))][\mathbf{P}_{N-1}(t) - \mathbf{P}(r_{N-2},t)] + (G_{N-1}(r)/G_{N-1}(r_{N-1}))[\mathbf{P}(r_{N-1},t) - \mathbf{P}_{N-2}(t)], \tag{16c}$$

for $r_{N-2} \leqslant r \leqslant r_{N-1}$.

Since the coordinate curves in the r variable are parabolic in each component and on each interval in Eq. (16), a resonable expectation would be for the curve to have no inflection points within an interval. To prove this assertion, the tangent vector must be computed. The natural unnormalized tangent vectors are given by the r derivative. When the r derivative of Eq. (16) is taken along with corresponding substitutions from Eqs. (11) and (12), the result is given by

$$\frac{\partial \mathbf{P}}{\partial r} = \frac{2}{h_m}\left\{[\mathbf{P}_{m+1}(t) - \mathbf{P}(r_m,t)] + \left(\frac{r-r_m}{h_m}\right)[\mathbf{P}(r_{m+1},t) - 2\mathbf{P}_{m+1}(t) + \mathbf{P}(r_m,t)]\right\}, \tag{17}$$

for $r_m \leqslant r < r_{m+1}$ and $m = 1, 2, \ldots, N-1$. A graphical illustration is given in Fig. 5, where the scaled derivative $(h_m/2)(\partial \mathbf{P}/\partial r)$ is decomposed into the two components of

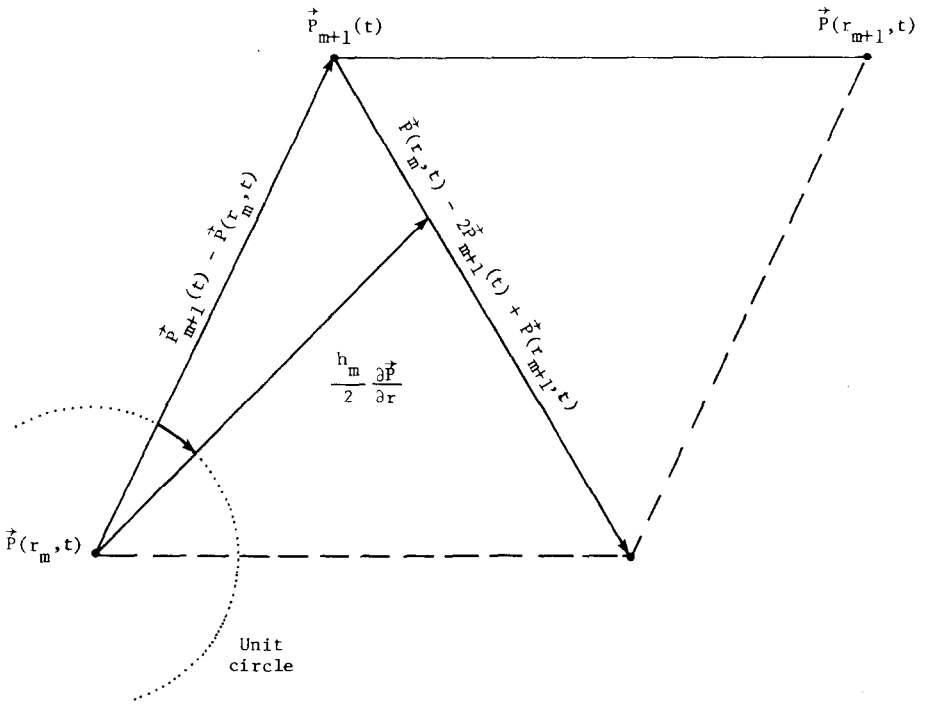

FIG. 5. Component decomposition of the derivative.

Eq. (17). The first component, $\mathbf{P}_{m+1}(t) - \mathbf{P}(r_m, t)$, is just a tangent vector at the point r_m. The second component, $\mathbf{P}(r_m, t) - 2\mathbf{P}_{m+1}(t) + \mathbf{P}(r_{m+1}, t)$, points in the discrete normal direction, or in other words, towards the concave side of the piecewise linear curve locally defined by $\mathbf{P}(r_m, t)$, $\mathbf{P}_{m+1}(t)$, and $\mathbf{P}(r_{m+1}, t)$. When the second component is scaled by $(r - r_m)/h_m$ and added to the first component, the scaled derivative is represented by the vector originating at $\mathbf{P}(r_m, t)$ and ending on the second component at its scaled length. Now, as r varies from r_m to r_{m+1}, the head of the scaled derivative vector moves linearly in r from the tail to the head of the second component. The rate at which the scaled derivative vector rotates as the curve is traversed with increasing r is best measured when it is normalized to unit length. Under the normalization, only unit tangent vectors to the curve are examined; rotation is then the only possible motion. In Fig. 5, the collection of unit tangent vectors is represented by the points on the unit circle centered about $\mathbf{P}(r_m, t)$. The curved arrow along the circle in Fig. 5 gives the total angular rotation that the tangent vector, given by the scaled derivative, has traversed. It should be clear that the rotation is monotone in r, hence, in curve arc length, since r is monotonically related to arc length. When $\mathbf{P}(r_m, t)$, $\mathbf{P}_{m+1}(t)$, and $\mathbf{P}(r_{m+1}, t)$ are not collinear, there is strict monotonicity, and the coordinate curve in r bends uniformly with the same direction of concavity as a circular arc approximation to the original noncollinear points with center at the arrow head of the discrete normal vector emanating from $\mathbf{P}_{m+1}(t)$ in Fig. 5. When the points are collinear, the coordinate curve in r degenerates to a straight line since the discrete normal vector, which is an approximation to a scaled second derivative, vanishes. As a result, there is no angular motion, reflected by the fact that there would be only one point on the unit circle to represent all unit tangent vectors for the curve segment. In formal terms, the curvature of the coordinate curves in r is just the arc length rate of change of the total angular rotation displayed in Fig. 5. To reexpress the conclusions, the coordinate curves in r for $r_m \leqslant r < r_{m+1}$ have strictly positive curvature in the noncollinear case and vanishing curvature in the collinear case. In the noncollinear case, the maximum curvature occurs when the actual tangent vector (Eq. (17)) is perpendicular to the discrete normal vector. In Fig. 5, perpendicularity leads to a tangent vector of minimal length and a discrete normal with a maximal projection onto tangent vectors of the unit circle. The minimal length for curve tangents means that the arc length derivative of r is maximal. The maximal projection for the discrete normal, and hence the second derivative, means that the rate of rotation is greatest. But the curvature is then just the product of these two quantities, each of which is maximal at the point of perpendicularity; hence, the curvature itself is maximal there.

In continuation, the osculating circle, defined as the tangent circle with matching second derivatives, has a center on the concave side of the curve measured from its point of contact with the curve. As r varies from r_m to r_{m+1}, the centers of the osculating circles all lie on the same side of the curve as does the center of the above mentioned circular approximation determined from the discrete normal vector. The result is that the coordinate curves in the r variable share the same convexity properties as the data determined by the intermediate surfaces for a fixed parameter t.

Such curves are called coconvex approximations to the data. In addition to the coconvex property, the curve also preserves existing monotonicity in the data, as can be witnessed by observation of Fig. 5 and the accompanying discussion. An illustration of a sample curve, with the properties discussed, is given in Fig. 6. The coordinate evaluations at partition points and the strict convexity within the intervals determined by partition points is evident from Fig. 6. Also evident from Fig. 6 is the potential change in convexity at a partition point r_m. Formally speaking, inflection points can occur at partition points r_m because the second r derivative is undefined there, except in certain cases when the curve locally degenerates to a single segment. The second derivative, rather than the curvature, is the critical measure for the type of inflection considered. To see why, consider a composite curve formed by the arcs of two distinct unit circles which are joined together at a point of tangency. Clearly, the composite curve has a continuous first derivative and a continuous curvature which is unity. But it has a discontinuous second derivative at the juncture between circles where, like the junctures for variable r coordinate curves, there is a change in concavity, an indication that the juncture is an inflection point. In another context, G. M. Nielson [16] used curves with continuous curvature but with discontinuous parametric second derivatives to formulate his splines with distributed tension. In addition to the convexity properties, the tangent vectors to the coordinate curves in r are nonvanishing and continuous for all r, including the inflection points. The tangent properties come from the multisurface interpolation (Eq. (1)) with continuous (C^0) interpolants (Eq. (11)) and is illustrated in Fig. 6. The continuous nonvanishing tangent vectors should not be taken entirely for granted, since curve continuity even up to second derivatives alone would not guarantee the result. To illustrate the point, consider the absolute value function $y = |x|$ in the parametric form given by $(-x^4, x^4)$ for $x \leqslant 0$ and (x^4, x^4) for $x > 0$. Parametrically, the curve belongs to class C^2 but has a slope discontinuity and a vanishing tangent at $x = 0$.

With the characteristics of the coordinate curves in r established above, the next task is to examine uniformity in the distribution of coordinate surfaces defined by

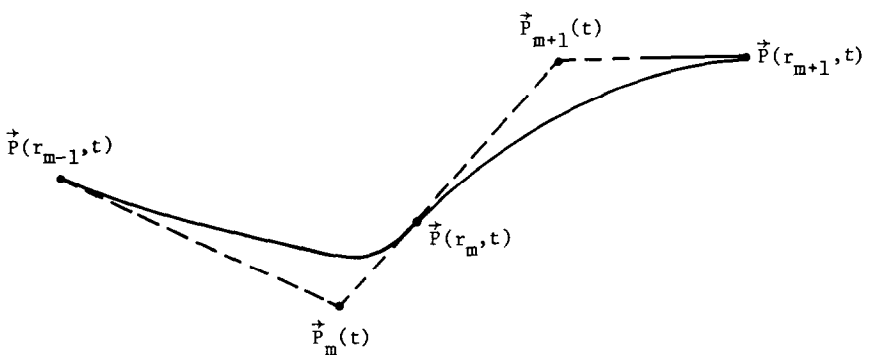

FIG. 6. Two segments of a coordinate curve in the r variable corresponding to the intervals $r_{m-1} \leqslant r < r_m$ and $r_m \leqslant r < r_{m+1}$, respectively.

constant values of r. By direct substitution from Eq. (11) into Eq. (10) of Theorem 1, the interpolation functions are clearly seen to be admissible. From Eqs. (11) and (12), the discrete projections defined by Eq. (5b) and given in Eq. (9) become

$$C_1(t) = b(t)\, h_1/2(r_{N-1} - r_1), \tag{18a}$$

$$C_k(t) = b(t)(h_{k-1} + h_k)/2(r_{N-1} - r_1), \tag{18b}$$

for $2 \leqslant k \leqslant N-2$; and

$$C_{N-1}(t) = b(t)\, h_{N-2}/2(r_{N-1} - r_1), \tag{18c}$$

in correspondence with the summary of Theorem 1. When the partition points $r_1 < r_2 < \cdots < r_{N-1}$ and/or when the intermediate control surfaces in the multisurface transformation (Eq. (2)) are selected so that the discrete projections satisfy Eq. (18), then the transformation distributes its constant r surfaces uniformly in a global manner. When two or more successive equations in Eq. (18) are satisfied, the uniformity is obtained locally. For example, if $C_m(t)$ and $C_{m+1}(t)$ are given by Eq. (18), then Eq. (13) yields a uniform distribution of constant r coordinate surfaces between $\mathbf{P}(r_m, t)$ and $\mathbf{P}(r_{m+1}, t)$ from Eq. (14) as r varies from r_m to r_{m+1}.

For a fixed parameter t, the multisurface transformation reduces to a curve approximation or interpolation algorithm. When $\tau(t)$ in Eq. (4) is selected to define a horizontal axis of a Cartesian system and when global uniformity from Eq. (18) is applied, a standard functional representation is obtained for the curve with r uniformly distributed along the horizontal axis. An approximation to the constructive surfaces $\mathbf{P}_1(t)$, $\mathbf{P}_2(t)$,..., $\mathbf{P}_N(t)$ is then a direct result in the approximation of functions. When the data is taken as the multisurface evaluations $\mathbf{P}(r_1, t)$, $\mathbf{P}(r_2, t)$,..., $\mathbf{P}(r_{N-1}, t)$ rather than the constructive surfaces, then an interpolation is obtained. If the intermediate surfaces are properly chosen, then the interpolation preserves the monotonicity and convexity of the given data. For this choice, the alpha-algorithm given by McAllister *et al.* [17] can be applied. When their $\frac{1}{2}$-algorithm is applied along with point insertion, the interpolation then reduces to the case that they presented in [18].

Coordinate Systems about Airfoils

With the local interpolants, precise local controls were formally established for the multisurface transformations. The controls provided the power to prescribe many important mesh properties. To demonstrate this power in an explicit sense, an illustrative sequence of meshes is given here. For simplicity, each is generated about a NACA0012 airfoil that is of unit length and with leading edge pointed in a negative x-direction.

In the first case, the airfoil is symmetrically surrounded by a box with 4 units in length, 2 in height and with circular arcs of radius 0.25 to round the corners. Along

the airfoil, a pointwise distribution is prescribed to cluster points at both leading and trailing edges. Along the box, a uniform pointwise distribution is prescribed. In addition to these distributions, the mesh properties are to also include orthogonality at both boundaries, a uniform distribution of coordinate curves above and below the airfoil, a progressively more rapid bending of coordinate curves on approaching the trailing edge, and a constant rate of entry into the box. All of the properties listed here are obtained with just $N = 5$ constructive surfaces $\mathbf{P}_k$ in Eq. (2) with partition points $r_k = (k-1)/(N-2)$. On the approach to the trailing edge, a polarlike system is more closely approximated if the coordinate curves which leave the airfoil become progressively flatter. The flatness is achieved when the curve is forced to bend into a line at a close distance from the airfoil. To accomplish the desired progressive bending, the first control surface $\mathbf{P}_2$ is selected to coincide with the airfoil $\mathbf{P}_1$ at its trailing edge, to gradually depart from the airfoil in going over it, to be at a maximum distance at the halfway point, then to go under the airfoil, and to gradually return to the trailing edge. The selection here is given by

$$\mathbf{P}_2(t) = \mathbf{P}_1(t) + 0.15(S(t)/S_{\max})[1 - (S(t)/S_{\max})]\,\hat{n}_1(t), \tag{19}$$

where $\hat{n}_1$ is the outward unit normal from the airfoil, $S(t)$ is the airfoil arc length as a function of the surface parameter, and $S_{\max}$ is the total arc length of the airfoil. The surface parameter t leads to the pointwise distributions, is taken to go from 0 to 1, and yields a counterclockwise orientation for the constructive surfaces. Moreover, its direct use for $\mathbf{P}_2$ in Eq. (19) causes an orthogonal alignment with points on $\mathbf{P}_1$. Had $\mathbf{P}_2$ been parameterized by $\mathbf{P}_2(f(t))$ for some nonlinear monotone function f, then there would have been no such alignment. For orthogonality at the box $\mathbf{P}_5(t)$, the control surface $\mathbf{P}_4(t)$ is defined by

$$\mathbf{P}_4(t) = \mathbf{P}_5(t) - 0.125\hat{n}_5(t), \tag{20}$$

where $\hat{n}_5$ is the outward unit normal field from the box. The constant displacement of 0.125 yields a uniform rate of entry into the box. The parameter t is the normalized box arc length that starts with the value of 0 at the positive x-axis, traverses the box

aligned along the positive x-axis and both box and airfoil are given the same orientation. To obtain exact local linearity for coordinate curves connecting airfoil to box, the inner control surface $\mathbf{P}_3$ is defined by the average

$$\mathbf{P}_3(t) = \tfrac{1}{2}[\mathbf{P}_2(t) + \mathbf{P}_4(t)], \tag{21}$$

with the indicated parametric correspondence. The resultant linearity occurs for values of r between $r_2 = \frac{1}{3}$ and $r_3 = \frac{2}{3}$. The earlier parametric alignment gives orthogonality at the airfoil when $r = r_1 = 0$ and at the box when $r = r_4 = 1$. In addition, because of the factors 0.15 in Eq. (19) and 0.125 in Eq. (20), there is a rough approximation to the uniformity conditions of Eq. (18) both above and below

the airfoil. Specifically, the spacing of control surfaces in the regions is in a nearly 2:1 ratio in leaving boundaries and is precisely 1:1 in the center. The resulting mesh is displayed in Fig. 7. On inspection, the specified mesh properties from the controls are evident.

With the boundary properties, the system for an airfoil in a box can be stacked in periodic alignment to produce a composite mesh that has continuous derivatives and which can be used to study cascades of unstaggerd airfoils. To include stagger, the airfoil must be rotated by a stagger angle and the box must be appropriately deformed. For this example, the same 5-surface format is used. The airfoil $\mathbf{P}_1$ and the first control surface $\mathbf{P}_2$ are rotated by a stagger angle of 45°. The box is deformed into a contour composed of successive line segments and circular arcs that parallel the airfoil camber line above and below the airfoil and which is smoothly capped at each end by half boxes. A gap of 1 between airfoils is specified with the top and bottom of the deformed box taken as 0.5 units both above and below the airfoil. Extensions both in front and in back are chosen also to be at one half the gap which is 0.5 units. From the deformed box $\mathbf{P}_5$, the control surfaces $\mathbf{P}_4$ and $\mathbf{P}_3$ are prescribed as before. To reflect the decrease in gap by a factor of two from the pure box example, the constants 0.15 and 0.125 appearing in Eqs. (19) and (20) are each divided by two. With a replacement of the independent variable r by a distribution function, a concentration of the mesh is specified near the airfoil. Along the airfoil surface, the mesh is clustered at leading and trailing edges with the trailing edge cluster being greatest on the bottom to push points into parametric alignment with the exit boundary. The rotated airfoil in the deformed box is then stacked in periodic alignment and extended both upstream and downstream by Cartesian systems. The resulting mesh is continuously differentiable everywhere and is displayed in Fig. 8. On examination, the mesh is seen to cover everything except two triangular regions that are bounded by distinct coordinate systems. From the periodic line, the Cartesian systems contain the distribution obtained from horizontal projections of

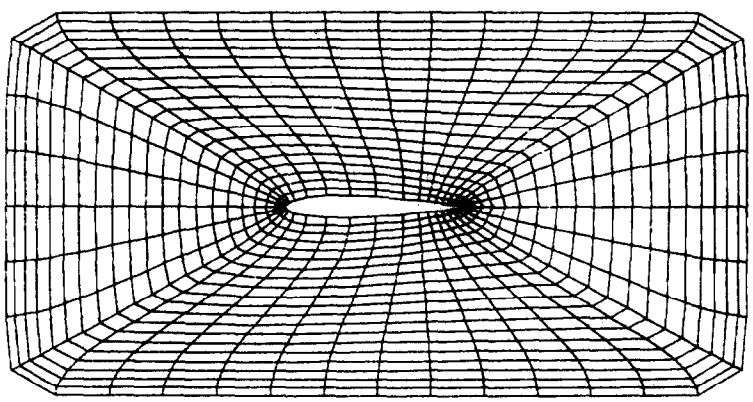

FIG. 7. Coordinates for an airfoil in a box.

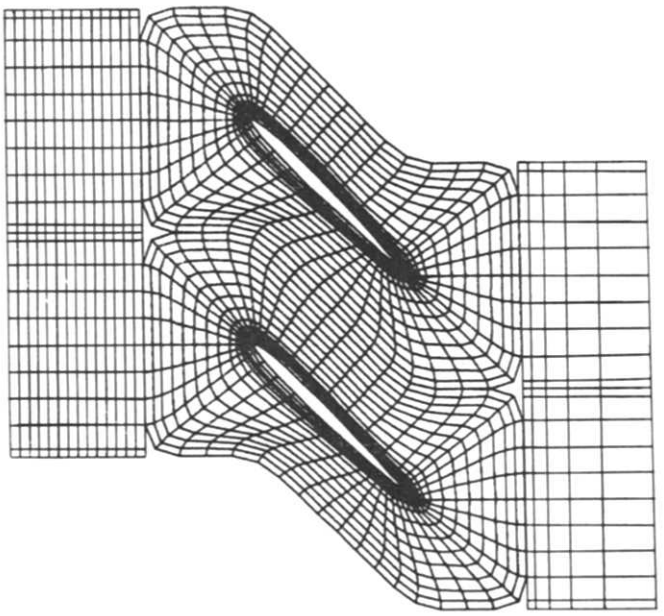

FIG. 8. A composite coordinate mesh for a cascade of airfoils with 45° stagger.

points along the circular arcs which border the triangular regions. The resultant Cartesian system is then distributed sinusoidally from the periodic line to smoothly join a uniform distribution for the remainder. Unlike previous cascade meshes, this composite system can be used for highly staggered closely spaced airfoils and has the clear advantage of the independent upstream and downstream Cartesian systems. Without the composite system, severe mesh distortion or growth would occur at even modest upstream and downstream extensions, regardless of which transformation method is used. The utilization of distinct coordinate systems has presented a topological problem which is clearly independent of the method of generation for each and which is reflected in the uncovered triangular shaped regions that resulted from the concurrent demand for nonsingularity. Such a composite system is obviously to be applied only when the uncovered regions are sufficiently small and/or are located in places where the solution is mild. An alternative approach is to relax the demand for nonsingularity and fill in the uncovered regions. In such a case, the system which loops around the airfoil would have singularities at some boundary corners which would propagate inward. With the use of several additional control surfaces, the inward propagation can be arbitrarily restricted to a region close to the distorted box while the previously prescribed mesh structure is retained. The local dependence on the control surfaces yields the power to create the desired restriction that can be taken to occur before the first inward mesh point. This effectively keeps the singularities from propagating inward.

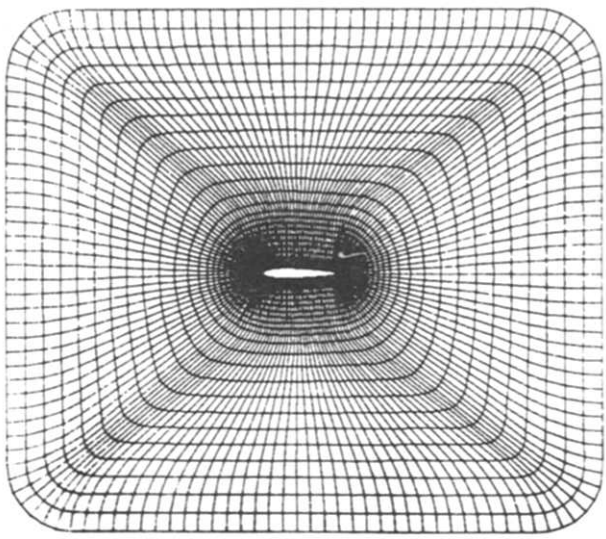

FIG. 9. Coordinates for an airfoil in a box with a local orthogonal disk around the airfoil.

Rather than pursue restrictions on the propagation of singularities, the several additional control surfaces will be used here to embed a desirable mesh structure within the global mesh. For this example, the original box format is considered again and the airfoil is now also to be surrounded by a local orthogonal system that smoothly deviates from orthogonality to meet the box with the previous mesh form. To form the local orthogonal system, three control surfaces replace a previous single surface and are given as uniform expansions in the outward normal directions from the airfoil. Orthogonal parametric alignment is prescribed as in Eq. (20) and the spacing is taken to satisfy the uniformity conditions of Eq. (18). With a subsequent clustering transformation for the r variable, the mesh is displayed in Fig. (9). The orthogonal region is observed to cover the locations where the significant fluid dynamic properties are typically expected to occur.

SUMMARY

Powerful local controls have been developed for mesh generation with the class of multisurface coordinate transformations. The controls come from local piecewise linear interpolants, and the resulting coordinates have continuous first derivatives. At boundaries, the mesh controls bring the capability to join distinct coordinate systems together with continuous derivatives. On regions in an area sense, mesh controls permit specifed structures to be smoothly embedded. Of paramount importance for area specifications are the uniformity controls that were derived in general for both global and local distributions of transverse coordinate curves. Applications of the

controls were given here by an illustrative sequence of two-dimensional examples. To consider general three-dimensional applications, however, at least two continuous derivatives are needed in order that the coordinate curves will bend continuously. Otherwise, undesirable creases could arbitrarily occur on coordinate surfaces. In a companion study [13], the local theory is extended to include the higher level of derivative continuity that is necessary to prevent problems such as the occurence of creases. In correspondence with the overall theory, a mesh generation software system has also been constructed under NASA Contract NAS3-22117.

REFERENCES

1. D. C. IVES, *AIAA J.* **14** (1976), 1006.
2. R. T. DAVIS, *in* "Proceedings, 4th AIAA Computational Fluid Dynamics Conference, p. 180, Williamsburg, V, July 24–26, 1979."
3. J. F. THOMPSON, F. C. THAMES AND C. W. MASTIN, *J. Comput. Phys.* **24** (1977), 274.
4. F. C. THAMES, J. F. THOMPSON, C. W. MASTIN AND R. L. WALKER, *J. Comput. Phys.* **24** (1977), 245.
5. J. F. THOMPSON, F. C. THAMES, J. K. HODGE, S. P. SHANKS, R. N. REDDY AND C. W. MASTIN, *in* "Fifth International Conference on Numerical Methods in Fluid Dynamics," p. 421, Springer-Verlag, Berlin, 1976.
6. H. HAUSSLING, *J. Comput. Phys.* **30** (1979), 107.
7. J. STEGER, AIAA Paper 77–665, Albuquerque, N.M., 1977.
8. U. GHIA, K. GHIA AND C. STUDERIUS, *in* "Fifth International Conference on Numerical Methods in Fluid Dynamics," p. 197, Springer-Verlag, Berlin, 1976.
9. J. STEGER AND R. SORENSON, *J. Comput. Phys.* **33** (1979), 405.
10. P. R. EISEMAN, *J. Comput. Phys.* **33** (1979), 118.
11. P. R.EISEMAN, *J. Comput. Phys.* **26** (1978), 307.
12. P. R. EISEMAN, *in* "Proceedings, 4th AIAA Computational Fluid Dynamics Conference," p. 166. Williamsburg, V., July 24–26, 1979."
13. P. R. EISEMAN, *J. Comput. Phys.* **47** (1982), 352.
14. G. FIX AND G. STRANG, "An Analysis of the Finite Element Method," Prentice–Hall, Englewood Cliffs, N.J., 1973.
15. D. LAUGWITZ, "Differential and Riemanian Geometry," Academic Press, New York, 1965.
16. G. M. NIELSON, *in* "Computer Aided Geometric Design" (R. Barnhill and R. Riesenfeld, Eds.), p. 209, Academic Press, 1974.
17. D. F. MCALLISTER, E. PASSOW AND J. ROULIER, *Math. Comput.* **31** (1977), 717.
18. D. F. MCALLISTER AND J. ROULIER, *Math. Comput.* **32** (1978), 1154.